Ultrafast Relaxation Dynamics Observed Through Time-Resolved Photoelectron Angular Distributions[†]

Julien Lecointre, Gareth M. Roberts, Daniel A. Horke, and Jan R. R. Verlet*

Department of Chemistry, University of Durham, South Road, Durham, DH1 3LE, U.K.

Received: March 31, 2010; Revised Manuscript Received: June 11, 2010

Time-resolved photoelectron imaging of the 7,7,8,8-tetracyanoquinodimethane (TCNQ) radical anion is presented. Photoelectron angular distributions (PADs) are qualitatively analyzed in terms of the simple s-p model that is based on symmetry arguments. The internal conversion dynamics from the first excited state (1^2B_{3u}) to the ground state ($^2B_{2g}$) may be observed through temporal changes in the PADs of the spectrally overlapping photoelectron features arising from photodetachment of the ground state and the excited state. A formulism for extracting the population dynamics from the β_2 anisotropy parameter of overlapping spectroscopic features is presented. This is used to extract the lifetime of the first excited state, which is in good agreement with that observed in the time-resolved photoelectron spectra.

I. Introduction

With the advent of commercial femtosecond lasers, time-resolved spectroscopy has provided unprecedented insight into the real-time dynamics of the electronic and geometric structure of molecules as they undergo reactions.[1] In its most commonly applied form, a femtosecond pump pulse initiates a reaction, and a delayed femtosecond probe pulse monitors the evolution of the excited system as it decays. The extent of information that can be retrieved is often determined by the choice of the probe pulse and the subsequent detection scheme. In the gas-phase, one of the most general detection schemes is time-resolved photoelectron spectroscopy (TRPES), in which the probe pulse removes an electron from the system and its kinetic energy reflects the excited state dynamics as the system evolves.[2] Its generality is mostly related to the fact that photoelectron spectroscopy (PES) does not adhere to stringent selection rules unlike most optical detection methods. Both bright states and dark states can be observed, and PES can provide high spectral resolution through techniques such as zero-kinetic energy spectroscopy,[3] as well as high temporal resolution using TRPES.[2] A particularly appealing feature of TRPES is that it can probe the dynamics along the entire reaction coordinate, as it is not restricted by Franck−Condon overlap. The main requirement following the photoionization of a neutral is that the cation formed must have an electronic configuration that corresponds to the neutral with the ejected electron removed.[2,4] As a result, the cation will often be in an excited electronic state following ionization. Because different electronic states in the neutral will correlate to different electronic states of the ion, these Koopmans' correlations can be used to monitor subtle dynamics through changes in the measured electron kinetic energies with time.[4]

Arguably, the most successful application of TRPES has been in the study of anions.[2,5] As the energy required to remove an electron is generally lower than for neutrals (or cations), both the ground and excited states may be monitored simultaneously.[6] Consequently, population decay may be tracked from the ini-
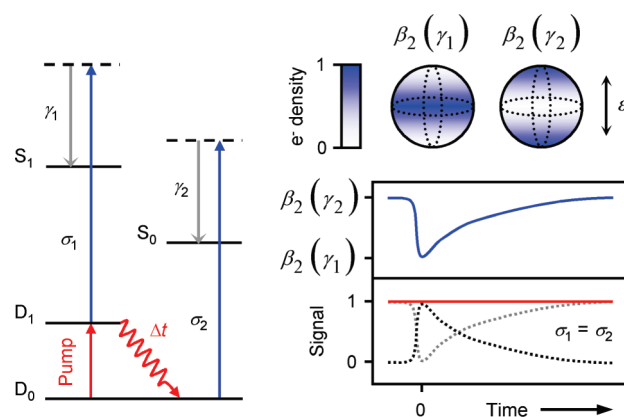

Figure 1. Example of a temporally evolving anion system, following excitation with a laser pump pulse (red arrow), which gives rise to two isoenergetic photoelectron features, γ_1 and γ_2 (gray arrows), after photodetachment (blue arrows), with associated detachment cross sections, σ_1 and σ_2, respectively. D_0 and D_1 are the doublet ground and excited states of the anion, respectively, and S_0 and S_1 are the singlet ground and excited states of the neutral. Shown inset are the photoelectron anisotropies associated with the two detachment features, $\beta(\gamma_1)$ and $\beta(\gamma_2)$ (ϵ is the laser polarization vector). The temporal evolution of the measured anisotropy (upper panel, solid blue line) and the observed signal for the isoenergetic features (bottom panel, solid red line) are shown when $\sigma_1 = \sigma_2$. The evolution of the D_0 and D_1 state populations are also shown on the bottom panel (gray and black dotted lines, respectively).

tially prepared excited state to the final state via any intermediate states. There is currently an ongoing effort in using laser sources based on high-harmonic generation to perform similar experiments in neutrals.[7] Despite the obvious advantages of such a methodology, it does require that Koopmans' correlations are favorable. As both the ground and excited state photoelectron features are varying with time, there is a requirement that these can be spectrally resolved. However, accidental isoenergetic photoelectron features may arise.[8] As an example, depicted in Figure 1, this may occur when: the anion excited state (D_1) correlates with an excited state in the neutral (S_1); the anion ground state (D_0) correlates with the neutral ground state (S_0); and the energy separation between the ground and excited states in the anion and neutral are similar, $E(D_0 \rightarrow D_1) \approx E(S_0 \rightarrow S_1)$.

Ultrafast Relaxation Dynamics

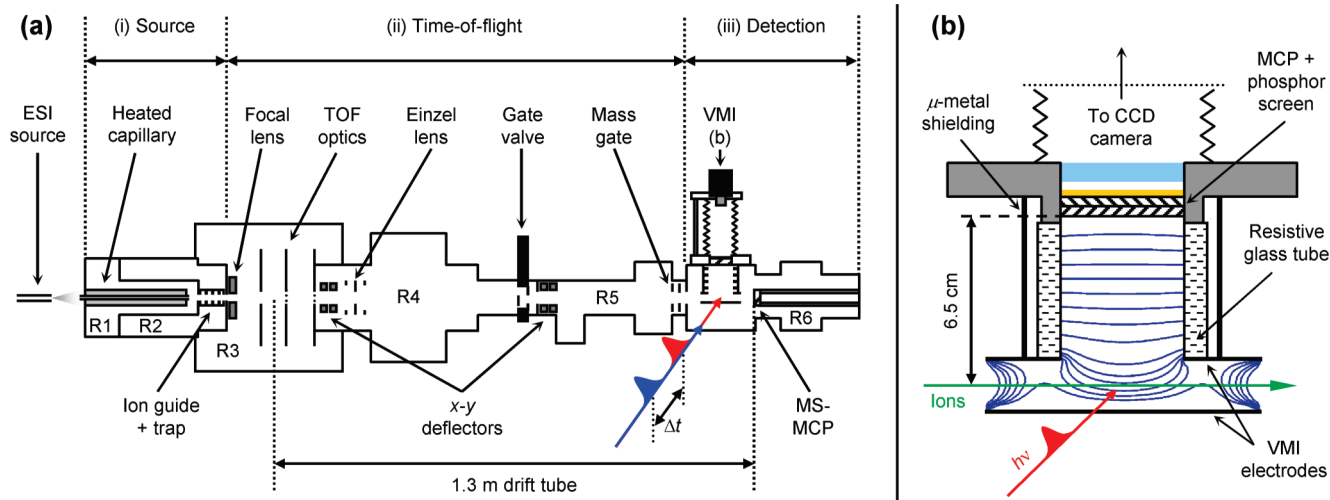*J. Phys. Chem. A, Vol. 114, No. 42, 2010* **11217**

Figure 2. (a) A schematic of the photoelectron imaging spectrometer that incorporates an electrospray ionization (ESI) source and a novel velocity map imaging (VMI) detector arrangement. Pump and probe laser pulses, separated by a time delay Δt, are shown by red and blue arrows, respectively. (b) Schematic of a new compact VMI detector arrangement. The detector is comprised of a resistive glass tube, a pair of μ-metal VMI electrodes and μ-metal magnetic shielding. The ion beam trajectory (green arrow), laser beam path (red arrow), and the electric field lines (blue lines) as calculated by Simion 8.0 are also shown. Figures 2a and 2b are explained in detail in the text.

In this case, the internal conversion from the D_1 state to the D_0 state would lead to isoenergetic photoelectron features γ_1 and γ_2. Spectrally overlapping features present a particular problem in larger molecular systems for which photoelectron peaks are typically very broad, such as those observed in the TRPES of benzene following excitation to the S_1 state.[9] In the worst case, if the two features are isoenergetic and their respective electron detachment cross sections are similar ($\sigma_1 = \sigma_2$), then the relaxation dynamics cannot be observed through TRPES. As TRPES effectively measures state populations, when the excited state decays (black dotted line in Figure 1) and the ground state concomitantly recovers (gray dotted line), the total observed photoelectron signal will not change (solid red line), hence additional information is required to extract the time scales of the dynamics.

Time-resolved photoelectron imaging (TRPEI) yields photoelectron velocity spectra.[10] These provide not only the electron kinetic energy but also angular information concerning the ejection angle of the electron relative to the photoionization field polarization, ϵ. The resultant photoelectron angular distributions (PADs) provide information about the orbital from which the electron was removed.[10,11] As the ground and excited state orbitals in TRPEI experiments typically differ, it may be anticipated that the respective PADs of the isoenergetic features also differ as depicted by $\beta(\gamma_1)$ and $\beta(\gamma_2)$ in Figure 1. In such a case, the relaxation dynamics may in principle be monitored using the time-dependent changes in photoelectron anisotropy (blue line, Figure 1) as population is transferred from one electronic state to another. TRPEI has been successfully applied to the study of rotational dynamics of molecules such as pyrazine[12] and C_2^-,[13] which reveal that PADs are particularly sensitive to molecular alignment. More recently, TRPEI has been used to gain insight into the adiabatic dissociation dynamics of prealigned CS_2 molecules, providing molecular-frame dynamics in which the temporally evolving PADs show the changing electronic character of the molecule as it evolves on the excited state.[14] Such experiments elegantly demonstrate the use of the additional information provided by PADs. Furthermore, full 3D alignment of polyatomic molecules has been demonstrated,[15] suggesting that there is scope for extending such methodologies to large polyatomic molecules. However, as molecular systems

become larger, the partial photoelectron waves that constitute the PADs rapidly increase in complexity, and it is generally only practical to qualitatively predict PADs.[10] Here, we show that subtle changes in the time-resolved PADs may be used to extract relaxation lifetimes for large molecular systems.

In recent years, there has been a drive to study larger systems such as conjugated organics,[9,16] DNA bases,[17] and other biologically significant molecules,[18] and in particular, anionic species that may be mass selected before being interrogated using PES. Using soft-ionization methods such as electrospray ionization (ESI),[19] the Wang group have demonstrated that PES can provide detailed electronic and molecular structure information for a vast class of molecules pertinent to organic and inorganic chemistry.[20] More recently, Kappes and co-workers have also performed TRPES on large complex molecules generated through ESI.[21] For example, the internal conversion dynamics were studied for the metal containing phthalocyanine-tetrasulfonate tetra-anion complexes, $[MPc(SO_3)_4]^{4-}$, where the free base complex (M = H_2) showed electron loss via tunneling through the repulsive Coulomb barrier.[21b]

In this article, an experiment designed to study large anionic molecules using TRPEI is described and a formulism for extracting population dynamics from time-evolving PADs is presented. In Section II, the experimental apparatus is described, which incorporates an ESI source and a novel velocity map imaging (VMI) design. In Section III we present time-resolved PADs of near isoenergetic features obtained from pump–probe experiments on the 7,7,8,8-tetracyanoquinodimethane (TCNQ) radical anion. Section IV presents an analysis of these photoelectron images and a method of extracting population dynamics. Finally, Section V presents a summary.

II. Experimental Details

Figure 2a presents a schematic overview of the instrument that is broadly divided into three major sections: (i) source region, (ii) time-of-flight (TOF) region, and (iii) detection region. Parts A–C of this section describe each of these in detail.

A. Source Region. Electrospray ionization (ESI) is used to generate isolated anions of interest. Unlike electron impact sources commonly used in TRPES experiments, ESI is a soft

ionization method and enables the generation of a wide range of large molecular species.[19] The ESI source itself consists of a stainless steel capillary (i.d. $\sim 100\ \mu m$). A 6 mM solution of TCNQ (Sigma-Aldrich) in acetonitrile is flowed through a PEEK transfer line from a quartz syringe (Hamilton 1000 series) using a syringe pump (World Precision Instruments, Aladdin 1000) at a flow rate of 250 $\mu L\ hr^{-1}$. The ESI capillary is biased to -3 kV and, as the solution exits the capillary, a divergent aerosol of negatively charged droplets is formed. The tip of the ESI source is placed at a distance of ~ 1 cm from the entrance of a stainless steel capillary (18 cm long and 600 μm i.d.), which is heated to ~ 80 °C using an aluminum block containing an embedded cartridge heater. This heated capillary acts as the interface between the ESI source, which operates at atmospheric pressure, and the first differentially pumped region of the instrument, labeled R1 in Figure 2a. R1 is evacuated to a pressure of ~ 1 Torr using a 100 $m^3\ hr^{-1}$ mechanical pump (Oerlikon, SV100B). The capillary is floated at a DC voltage, typically ~ -50 V, and is controlled by a homemade power supply, as are all subsequent DC voltages described in this part of Section II. Each output is floated on top of the next, with the heated capillary voltage being the last and largest in the chain.

After exiting the heated capillary into R1, anions pass through a pinhole (1 mm dia.), biased at -40 V, and enter a second vacuum region (R2). This second region is evacuated using a 250 L s^{-1} turbomolecular pump (Oerlikon, TW250S) to a pressure of ~ 5 mTorr, which may be controlled by limiting the conductance to the pump using a bellows sealed angle valve. The divergent anion beam then enters an ion guide, which is loosely based on the design described by Wyttenbach et al.[22] The ion guide has a two-fold purpose: (1) it radially confines and axially guides the anion beam exiting the aperture and (2) it creates an electrostatic trap in which anions can be accumulated. The ion guide consists of 33 stainless steel electrodes mounted between two printed circuit boards (PCBs), where each electrode has dimensions of 11.98 mm $\times$ 19.08 mm $\times$ 0.20 mm (width $\times$ height $\times$ thickness). All electrodes are equally spaced by 1.47 mm and have an axisymmetric hole at their center (3.2 mm dia.) to enable the passage of anions along its central axis. The first and penultimate electrodes of the device are placed at separate DC voltages (-35 and -20 V, respectively). A DC voltage ramp between these two voltages is generated using 1 MΩ surface mounted resistors between each of the electrodes. This ramp provides an axial potential gradient that pushes ions towards the end of the guide. Radial confinement is achieved by applying RF voltages (1$-$2 MHz, 100$-$250 V_{pp}) to the electrodes. Alternating electrodes have an RF applied which is out-of-phase from the previous. The pair of RF voltages are generated using a self-oscillating power supply (Ardara Technologies, PSRF-100) and are coupled to the DC ramp using 100 pF capacitors connected to each of the electrodes. The resistive chain and the coupling capacitors are surface mounted on the two PCBs, respectively.

ESI generates a continuous source of ions, while TRPEI is inherently pulsed because of the use of femtosecond lasers, which typically operate at a repetition rate in the kHz range. The ion guide also serves as a trap in which ions accumulate for ~ 1 ms, before they are extracted and injected into the next region. The final electrode is electrically isolated from the first 32 electrodes and may be pulsed using a fast voltage pulser. The trap is closed when its voltage (typically -50 to -80 V) is more negative than the voltage at the end of the ramp and open if less negative. It takes $\sim 2.5\ \mu s$ to empty the trap, and the continuous source is turned into a pulsed source with

minimal loss.[22] The primary source of ion loss in the current arrangement is from space-charge repulsion imposed by the relatively small dimensions of the trap. By tuning the amplitude of the RF voltages applied to the ion guide, a rough m/z range over which the funnel can efficiently trap anions can be optimized. The ions undergo many collisions in their passage through the ion guide and in the trap, such that ions will be in thermal equilibrium with the background gas, which is approximately room temperature (298 K).

B. Time-of-Flight Region. Unloading the trap accelerates an anion packet through a 1.8 mm diameter aperture into a third differentially pumped chamber (R3), evacuated to a pressure of 5×10^{-6} Torr using a 3000 L s^{-1} diffusion pump (Oerlikon, DIP3000). Upon entering this region of the spectrometer, the divergent anion packet is collimated into a colinear Wiley$-$McLaren (WM) TOF arrangement,[23] using a grounded tubular focal lens. Ions are injected into the TOF with an energy defined by the DC offset of the trap. By varying the voltage to which the trap is pulsed open, ions can be spatially focused into the center of the TOF optics (indicated in Figure 2a by the start of the drift tube). Ions pass through 5 mm apertures in the center of each of the three TOF electrodes. The last of these is grounded and defines the start of the 1.3 m field-free drift region and partitions R3 from the next differentially pumped region, R4. Ions are extracted into the drift region by applying high voltage pulses to the first (extractor) and second (accelerator) electrodes of the TOF optics (-2.3 kV and -1.9 kV, respectively). To prevent detrimental lensing effects as ions pass through the TOF arrangement, high transmission stainless steel mesh (TWP, Berkley CA, 88% transmission) has been placed over the apertures in the accelerator and ground TOF plates.

The fourth (R4) and fifth (R5) regions of the instrument are separated by a 5 mm diameter aperture and are pumped to pressures of 2×10^{-7} Torr and 1×10^{-8} Torr using a 250 L s^{-1} turbomolecular pump (Edwards, EXT250H) and a 150 L s^{-1} turbomolecular pump (Oerlikon, Turbovac 151), respectively. As ions travel through R4 and R5, they are spatially focused using a pair of Einzel lenses and aligned with two sets of x-y deflectors into the detection region of the spectrometer. The second Einzel lens, labeled as the mass gate in Figure 2a, is placed just before a final 5 mm diameter aperture leading into the detection region (R6). At very high negative voltage, the mass gate repels anions as they enter it, and by lowering the voltage at a given time delay from the TOF pulse to the optimal voltage required by the Einzel lens, a packet of ions with known m/z ratio is selected and focused into the laser interaction region.

Ions are detected using a pair of 40 mm diameter multichannel plates (MCPs) placed in the detection region, labeled MS-MCP in Figure 2a. In the case of TCNQ$^-$, the mass spectrum is dominated by a single peak at $m/z = 204$ amu. Using the known gain of the MCPs, we estimate that an ion packet on average contains $\sim 10^3$ ions.

C. Laser System and Detection Region. A commercial femtosecond laser system (Spectra-Physics, Spitfire XP-Pro), delivering 35 fs pulses centered at 800 nm (1.55 eV) with an energy of 3 mJ/pulse at 1 kHz, is used to generate pump and probe laser pulses. For experiments performed on TCNQ$^-$, a portion of the fundamental is used for pump pulses and has a bandwidth of ~ 30 nm (~ 60 meV). Probe pulses are generated by frequency doubling the 800 nm using a 300 μm thick type I β-barium borate (BBO) crystal. The 400 nm (3.10 eV) probe pulses are delayed relative to the pump pulses using an optical delay line controlled by a motorized delay stage (Physik-

Ultrafast Relaxation Dynamics

J. Phys. Chem. A, Vol. 114, No. 42, 2010 **11219**

Instrumente, M-505). Pump and probe beams are recombined and sent unfocused into the detection region through a CaF_2 window (1.5 mm thickness). The polarization of the laser electric field is set parallel to the plane of the imaging detector. Pump and probe beams have energies of 120 μJ/pulse and 70 μJ/pulse, respectively, and both have power densities of $\sim 1 \times 10^{10}$ W cm^{-2} at the interaction volume with the ion packet. The temporal width of the pulse pair has been determined to be $\sim$120 fs from their cross-correlation in a second thin BBO crystal.

An 80 L s^{-1} turbomolecular pump (Oerlikon, Turbovac SL-80) is used to evacuate the detection region (R6) to an operational pressure of 5×10^{-9} Torr. R6 houses the photo-electron velocity map imaging (VMI) detection arrangement, which is shown in greater detail in Figure 2b. A typical VMI arrangement oriented perpendicular to the ion beam axis with a design similar to that used by Eppink and Parker[24] would generate a potential difference of $\sim$250 V. This is sufficient to deflect the ion beam into the VMI electrodes before it reaches the laser interaction volume. In order to avoid this, the VMI electrodes may be rapidly pulsed. To avoid this extra complexity and the cost of high voltage pulsers and their control, the design presented here involves relatively low voltages and specifically avoids large electric fields, particularly in regions where the ion beam propagates.

Figure 2b shows our VMI arrangement, which consists of two μ-metal VMI electrodes, a resistive glass tube (Photonis) and an MCP + phosphor screen detector (Photek Ltd., VID240). The resistive glass tube is magnetically shielded with μ-metal tubing. The two VMI electrode plates (o.d. of 9.6 cm and a 1.0 mm thickness) are separated by 1.6 cm using stainless steel spacers and ceramic washers. The accelerator plate has a large opening at its center (3.9 cm dia.) that creates the inhomogeneous electric field that focuses the photoelectrons on the MCP, which is positioned 6.5 cm from the point of laser-ion interaction. The resistive glass tube, which is similar in principle to a single pore of an MCP, acts as an infinite chain of electrodes coupled to each other with a series of resistors. The resultant electric field (calculated using Simion 8.0 and shown as solid blue lines in Figure 2b) reduces chromatic aberrations from the lens and allows for the short flight-tube to be used without significant loss of resolution. This ultimately enables the use of low voltages on the extractor and accelerator electrodes. Both electrodes, biased at -250 V, image 5 eV electrons on the 40 mm diameter MCPs. The fact that both electrodes have the same voltage (to within $\sim$2%) results in very small deviations of the ion beam ($<1°$ for a 2 keV ion beam). The resolution is $\sim$5%, although we note that it was not designed specifically with high resolution in mind. It is also worth pointing out that the resistive glass tube employed here may find uses in other VMI arrangements where a series of resistors have been used to generate smoothly varying fields.[25]

The velocities of emitted photoelectrons (speed and angle) are projected onto the detector where the current is amplified by the MCPs. These are then accelerated to and impact on the phosphor screen from which emitted light is subsequently captured using a CCD camera (Basler, A312f). Photoelectron spectra are extracted from the raw photoelectron images, which are recorded over $\sim 10^5$ laser shots, by subtracting the superfluous azimuthal component using a polar onion-peeling algorithm developed in our group.[26] The spectra have been calibrated with the well-known photoelectron spectrum of iodide at 266 nm. The resolution of the VMI spectrometer is $\Delta E/E \approx 5\%$ or is limited by the bandwidth of the laser, which in the current experiments occurs below electron kinetic energies of $\sim$1.2 eV.
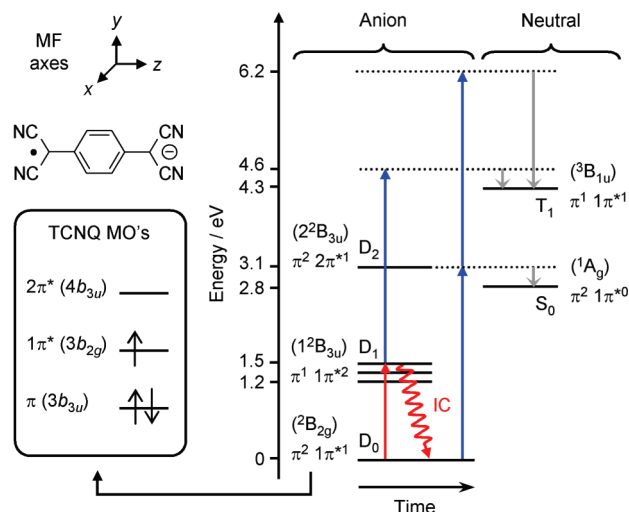

Figure 3. Energy level diagram for the 7,7,8,8-tetracyanoquinodimethane (TCNQ) radical anion (molecular structure shown inset) showing the temporal evolution of the D_1 excited state via internal conversion (IC) back to the D_0 ground state, following excitation at 1.5 eV (pump = red arrow, probe = blue arrow, electron kinetic energies = gray arrows). D_0, D_1, and D_2 correspond to the doublet states of the anion and S_0 and T_1 are the ground and first excited states of the neutral. Corresponding term symbols are show in parentheses with the state electron configurations below. Also presented inset are the valence molecular orbitals (MOs) of TCNQ with the D_0 state configuration shown (orbital symmetries are given in parentheses). The molecular-frame (MF) Cartesian axes assigned to TCNQ$^-$ are shown above its molecular structure.

PADs are obtained directly from the polar onion-peeling routine, in which they are extracted from fits to the angular distribution functionality:

$$\frac{d\sigma}{d\Omega} = \frac{\sigma}{4\pi} \sum_n \beta_n P_n(\cos\theta) \qquad (1)$$

where σ is the total photodetachment cross-section, $P_n(\cos\theta)$ are nth order Legendre polynomials, β_n are the anisotropy parameters and the factor 4π accounts for normalization over the solid angle, Ω. For a one-photon process, only even terms up to $n = 2$ need to be considered, whereas for a two-photon transition, the additional alignment induced by the first photon requires even terms up to $n = 4$. β_2 values range from $+2$ to -1, which correlates to photoelectron emission that is predominantly parallel or perpendicular to the polarization axis, respectively.

III. Results

TRPEI has been performed on the 7,7,8,8-tetracyanoquinodimethane (TCNQ) radical anion (structure shown inset in Figure 3) by utilizing pump and probe photon energies of 1.5 eV (800 nm) and 3.1 eV (400 nm), respectively. A schematic energy level diagram of the anionic and neutral states of TCNQ together with the pump–probe scheme is shown in Figure 3. D_0, D_1, and D_2 are the anion doublet ground state ($^2B_{2g}$) and excited states, 1^2B_{3u} and 2^2B_{3u}, respectively. S_0 and T_1 are the ground (^1A_g) and first excited ($^3B_{1u}$) states of the neutral. Also shown inset in Figure 3 is the energy ordering of the valence molecular orbitals (MOs) of TCNQ with their respective orbital symmetries shown in parentheses. The 1.5 eV pump excites TCNQ$^-$ from the D_0 ground state to the first excited D_1 state, by promoting a core electron from the π ($3b_{3u}$) orbital into the
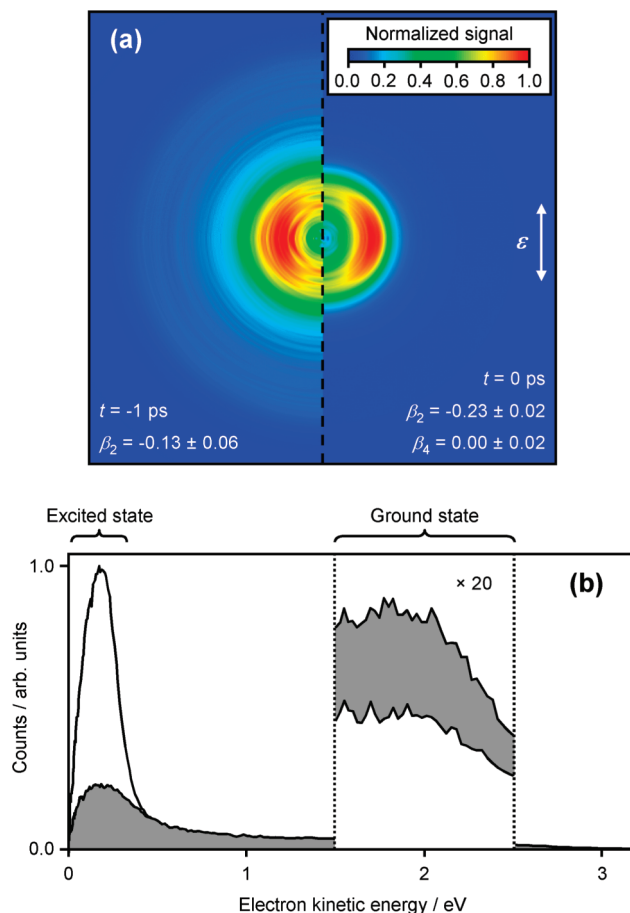
Figure 4. (a) Deconvoluted photoelectron images obtained from the time-resolved experiments performed on TCNQ⁻, using pump and probe energies of 1.5 eV (800 nm) and 3.1 eV (400 nm), respectively. The left half corresponds to an image recorded at $t = -1$ ps and the right half to an image recorded at $t = 0$ ps (laser polarization direction, ϵ, is also shown inset). Both raw images were acquired over 1.75×10^5 laser shots at 500 Hz. Also shown are the measured anisotropy parameters, β_n, for the low energy feature (0.2 eV) in both images. (b) Corresponding photoelectron spectra obtained from the images at $t = -1$ ps (gray) and $t = 0$ ps (white).

$1\pi^*$ ($3b_{2g}$) orbital. The probe pulse at 3.1 eV subsequently detaches an electron from either the excited or ground anion states.

Figure 4a shows deconvoluted photoelectron (PE) images acquired over 1.75×10^5 laser shots at 500 Hz and obtained at two different pump−probe delays: $t = -1$ ps and $t = 0$ ps. The corresponding PE spectra are shown in Figure 4b. When the probe pulse arrives before the pump pulse ($t = -1$ ps), the recorded PE image shows two distinct features: an intense sharp feature at small radii and a broader feature at larger radii. Both of these processes exhibit anisotropy with photoelectrons detached predominantly perpendicular to the laser polarization axis, ϵ ($\beta_2 < 0$). The low energy feature corresponds to the peak at 0.2 eV in the PE spectrum and arises when the 3.1 eV probe photon, which is resonant with the $D_0 \rightarrow D_2$ transition, excites TCNQ⁻ to the higher lying D_2 state. As the excited D_2 state is unbound with respect to the neutral ground state, the electron promptly undergoes autodetachment to form neutral TCNQ in the correlated S_0 ground state. The second feature, corresponding to the broad peak at ~2.0 eV in the PE spectrum, arises from a resonance enhanced two-photon detachment process from the D_0 ground state, via the D_2 state. Although the D_2 state has a dominant $\pi^2 2\pi^{*1}$ electron configuration, which correlates to the

neutral S_0 state following electron detachment from the $2\pi^*$ ($4b_{3u}$) orbital, we have shown that this state possesses a significant contribution from the $\pi^1 1\pi^{*2}$ configuration.[8] Detachment of an electron from the $1\pi^*$ orbital of the $\pi^1 1\pi^{*2}$ configuration of the D_2 state correlates to the T_1 state of the neutral, and it is this detachment process that gives rise to the PE feature observed at 2.0 eV.

When pump and probe are temporally overlapped ($t = 0$ ps) the pump pulse excites TCNQ⁻ into the D_1 state, concomitantly depleting population in the D_0 ground state. The recorded PE image shows a large increase in signal around 0.2 eV and depletion in the high energy 2.0 eV feature. The signal reduction in the latter peak is more clearly observed in the associated PE spectra shown in Figure 4b, and this feature is a direct measure of the D_0 state population. The increase in signal around 0.2 eV results from a new detachment process, which is assigned to the detachment of an electron from the $1\pi^*$ orbital in the D_1 excited state and generates neutral TCNQ in its electronically correlated T_1 state.[8] However, at this energy, there is also a feature arising from the D_0 ground state that is expected to decrease in intensity as some population has been transferred from the ground state. These two features are spectrally overlapping and therefore nearly isoenergetic.

The isoenergetic nature of the two features arises from the fact that the $D_0 \rightarrow D_1$ transition is similar in energy to the $S_0 \rightarrow T_1$ energy separation, $E(D_0 \rightarrow D_1) \approx E(S_0 \rightarrow T_1) = 1.5$ eV.[8] In the case of TCNQ⁻, these two features have very different detachment cross sections. The cross section for detachment from the D_1 excited state, σ^e, is much greater than the detachment cross section from the D_0 ground state, σ^g. As a result, changes in signal at 0.2 eV predominantly reflect excited state dynamics (hence the excited state label on the PE spectra in Figure 4b) and an internal conversion lifetime of $\tau = 650$ fs has been measured.[8] This is a rather fortunate case, and if the excited state and ground state detachment processes were to have similar detachment cross sections, $\sigma^g \approx \sigma^e$, the time-resolved PE spectra would not show temporal changes and the additional information concerning the PADs may be used to monitor the dynamics.

Comparison of the images obtained at $t = -1$ ps and $t = 0$ ps indicates that the PADs around the isoenergetic features at 0.2 eV change due to the change in relative contributions from the two detachment processes. Before $t = 0$, the detachment involves only a single photon, and the anisotropy may be quantified by β_2 only. The average anisotropy parameter over the spectral range from 0.15 to 0.25 eV is $\beta_2 = -0.13 \pm 0.06$. At $t = 0$, the excited state feature involves two photons and requires the additional β_4 term to describe the PAD. Measured anisotropy parameters for the isoenergetic feature at $t = 0$ are $\beta_2 = -0.23 \pm 0.02$ and $\beta_4 = 0.00 \pm 0.02$.

In Figure 5 the temporal evolution of the anisotropy parameters for these PE features around 0.2 eV are shown. Figure 5a shows the time-dependence of the β_2 parameter, which clearly indicates a change in the anisotropy when the D_1 excited state is populated at $t = 0$. The recovery of the β_2 parameter towards its value before $t = 0$ is indicative of a loss of population in the excited state through internal conversion back to the D_0 ground state. Figure 5b indicates that the higher order β_4 parameter is approximately zero and is time-independent. In both figures, the error bars represent the standard deviation. The time-variation of the β_2 anisotropy parameter, shown in Figure 5a for the isoenergetic features, suggests that it may be possible to extract the relaxation lifetime, τ, from the PADs alone.
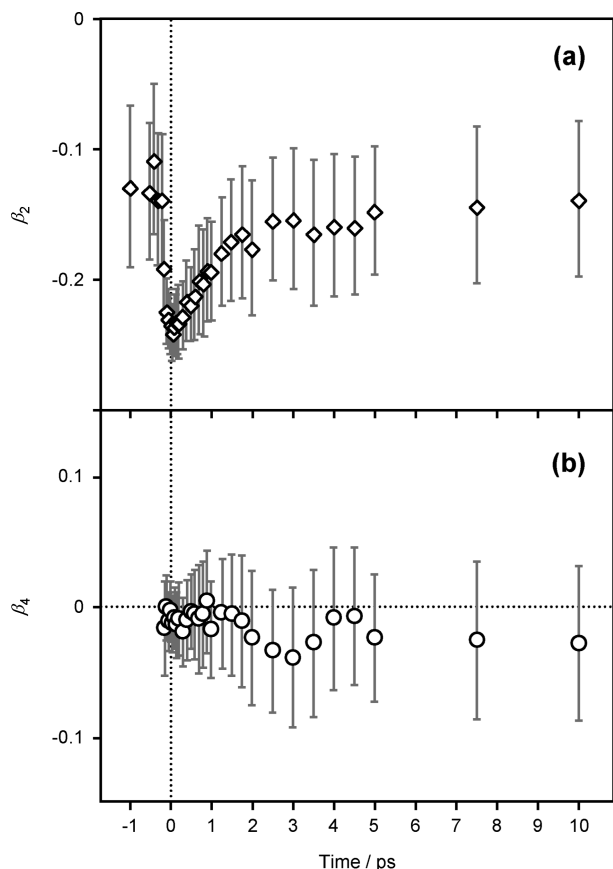
Ultrafast Relaxation Dynamics

J. Phys. Chem. A, Vol. 114, No. 42, 2010 **11221**

Figure 5. Temporal evolution of the measured β_2 (a) and β_4 (b) anisotropy parameters for the 0.2 eV photoelectron feature (see Figure 4). Error bars are shown in gray and correspond to one standard deviation.

IV. Analysis and Discussion

A. Photoelectron Angular Distributions. A distinct advantage of photoelectron imaging is that it provides direct access to PADs, which can be analyzed to yield information about the symmetries of the orbitals from which the electrons are removed.[27] Although for large molecular systems, such as TCNQ, it is generally difficult to extract quantitatively meaningful information, Sanov and co-workers have demonstrated an elegant qualitative method to gain insight into the detachment process for relatively slow photoelectrons.[10b] At low kinetic energies, the Wigner threshold law dictates that the outgoing PE wave is dominated by low angular momentum (l) partial waves, specifically, s- and p-waves ($l = 0$ and 1, respectively).[28] The so-called s-p model considers which symmetry components of these partial waves, $\Gamma(e^-)$, contribute to the total PE wave, given the symmetry of the orbital from which the electron is detached, $\Gamma(\psi)$, and the molecular-frame (MF) components of the transition dipole moment, $\Gamma(\mu_i)$, where i represents the Cartesian coordinate (see Figure 3 for a definition of MF Cartesian axes): $\Gamma(\psi) \otimes \Gamma(\mu_i) \otimes \Gamma(e^-) \supseteq \Gamma_{TS}$.

In the PE spectrum at $t = 0$, the PAD of the 0.2 eV feature is quantified by $\beta_2 = -0.23$, indicating that the PE waves are predominantly emitted perpendicular to the laser polarization axis, defined as the z-axis in the lab-frame (LF). This feature is dominated by the detachment from the D_1 to T_1 states. However, the D_1 state is prepared by excitation from the D_0 state. The allowed components of the transition dipole moment, μ_i, in the excitation step, are defined by the symmetries of the singly occupied MOs of the D_0 and D_1 states. Specifically, $b_{3u} \otimes \Gamma(\mu_i) \otimes b_{2g}$ must equal the totally symmetric irreducible

representation of the D_{2h} point group (a_g) that TCNQ$^-$ belongs to, which is only true for the z-component of the transition dipole moment ($\Gamma(\mu_z) = b_{1u}$). Hence, TCNQ$^-$ molecules that are excited in the D_1 state have their MF z-axis preferentially aligned parallel to the LF z-axis (polarization axis). Within the s-p model, detachment from the D_1 ($1\pi^*$), which is a b_{2g} orbital, is expected to yield PE waves perpendicular to the LF z-axis, yielding a negative anisotropy, in qualitative agreement with Figure 4a.

In the PE spectrum at $t = -1$ ps, the feature at 0.2 eV is generated by one-photon detachment from the D_0 to the S_0 ground state of the neutral. The detachment is either direct or occurs via the D_2 state, which promptly autodetaches to the S_0 state. For direct photodetachment, the s-p model predicts PE waves with a negative anisotropy. However, the gas-phase photodetachment spectrum, recorded by Brauman and co-workers, suggests that autodetachment is the dominant process.[29] In this case, the transition dipole moment from D_0 to D_2, $\Gamma(\mu_z) = b_{1u}$, preferentially aligns the MF z-axis of the excited TCNQ$^-$ along the LF z-direction. As the autodetachment is fast,[8] one might expect to see anisotropy from this. Specifically, the overall symmetry of the initial state must be maintained in the final state (neutral and electron). Given the D_2 state symmetry is b_{3u} and the neutral S_0 state, a_g, the symmetry of the outgoing wave is expected to be b_{3u}, which requires that it is ejected perpendicular to the LF z-axis, as is observed in Figure 4a. However, the above analysis is of course an oversimplification because of a lack of detailed knowledge concerning the electron-neutral scattering dynamics and given that the direct detachment may also interfere.

For the broad feature at 2.0 eV, which corresponds to detachment from the D_2 state to the T_1 state of the neutral, we extract anisotropy parameters $\beta_2 = 0.09 \pm 0.08$ and $\beta_4 = 0.00 \pm 0.07$. A similar analysis using the s-p model for this transition leads to an expected negative anisotropy, in contradiction to what is observed. This discrepancy highlights the main limitation of the model in that it is only valid in the limit of low electron kinetic energies where the low-l partial waves have relatively high cross sections.

B. Temporal Evolution of Photoelectron Angular Distributions. In Figure 5, the temporal evolution of both the β_2 and β_4 parameters are shown. The most prominent variation is observed in the temporal evolution of β_2, whereas β_4 is approximately zero and exhibits no significant time-dependence. The β_4 parameter describes the alignment induced by the pump pulse and its evolution predominantly reflects the rotational dynamics of the system.[13] For TCNQ$^-$, the rotational motion is much longer than that of the electronic relaxation dynamics and so in the analysis that follows we assume that β_4 is negligible.

It is convenient to define the anisotropy parameter in terms of the components of the cross-section parallel, $\sigma_\parallel$, and perpendicular, $\sigma_\perp$, to the laser polarization axis:

$$\sigma_\parallel = \frac{\sigma}{4\pi}[\beta_2 + 1]$$
$$\sigma_\perp = \frac{\sigma}{4\pi}[1 - (\beta_2/2)] \tag{2}$$

The expressions in eq 2 are obtained from eq 1 with the parallel and perpendicular components corresponding to $\theta = 0$ and $\theta = \pi/2$, respectively. Using this definition in eq 2, we may express β_2 in terms of the ratio $R = \sigma_\parallel/\sigma_\perp$,

$$\beta_2 = \frac{R - 1}{1 + (R/2)} \tag{3}$$

To extract β_2 from an image, the above definition is valid, although it is more accurate to fit the entire angular distribution using eq 1 as is done in the onion-peeling routine.[26] However, by defining β_2 in terms of relative cross sections, the effect of multiple contributions to the total observed signal may be considered in a more straightforward manner. For TCNQ$^-$, there are two features that are (near) isoenergetic. One originates from the photodetachment of the D_0 ground state and has an associated cross-section, σ^g, while the other from the photodetachment of the D_1 excited state with an associated cross-section, σ^e, as described in Section III. The observed signal, S^k, from each of these processes can then be expressed in terms of their respective cross sections:

$$\begin{aligned} S^g &\propto \sigma^g P^g \\ S^e &\propto \sigma^e P^e \end{aligned} \tag{4}$$

where P^k represents the fractional population in state k. As the excited state is a transient with lifetime τ, we may introduce the first order time-dependence associated with its decay and the concomitant recovery in the ground state:

$$\begin{aligned} S^g(t) &\propto \sigma^g[1 - \alpha \cdot \exp(-t/\tau)] \\ S^e(t) &\propto \sigma^e[\alpha \cdot \exp(-t/\tau)] \end{aligned} \tag{5}$$

where α is the fraction of molecules initially transferred to the excited state from the ground state by the pump pulse. The total signal is then simply the sum of the two components,

$$S(t) = S^g(t) + S^e(t) \tag{6}$$

When $\sigma^e = \sigma^g$, $S(t)$ becomes time-independent and the dynamics cannot be observed via the signal in the PE spectra alone. From eq 2, we may rewrite the observed signal in terms of the signal observed parallel and perpendicular to the laser polarization axis:

$$\begin{aligned} S_\parallel(t) &= S_\parallel^g(t) + S_\parallel^e(t) = \frac{1}{4\pi}[S^g(t)(\beta_2^g + 1) + S^e(t)(\beta_2^e + 1)] \\ S_\perp(t) &= S_\perp^g(t) + S_\perp^e(t) = \frac{1}{4\pi}[S^g(t)(1 - \beta_2^g/2) + S^e(t)(1 - \beta_2^e/2)] \end{aligned} \tag{7}$$

where β_2^k is the anisotropy associated with the photodetachment from state k. Substituting the relevant $S^k(t)$ from eq 5 into eq 7, the following expressions may be obtained:

$$\begin{aligned} S_\parallel(t) &\propto \alpha[\eta\beta_2^e + \eta - \beta_2^g - 1]\exp(-t/\tau) + [\beta_2^g + 1] \\ S_\perp(t) &\propto \alpha[\eta - \eta(\beta_2^e/2) + (\beta_2^g/2) - 1]\exp(-t/\tau) + [1 - (\beta_2^g/2)] \end{aligned} \tag{8}$$

where $\eta = \sigma^e/\sigma^g$. For the specific case of $\sigma^e = \sigma^g$, eq 8 reduces to:

$$\begin{aligned} S_\parallel(t) &\propto \alpha[\beta_2^e - \beta_2^g]\exp(-t/\tau) + [\beta_2^g + 1] \\ S_\perp(t) &\propto \frac{\alpha}{2}[\beta_2^g - \beta_2^e]\exp(-t/\tau) + [1 - (\beta_2^g/2)] \end{aligned} \tag{9}$$

Analogous to eq 3, we may now define $\beta_2(t)$ as

$$\beta_2(t) = \frac{R(t) - 1}{1 + (R(t)/2)} \tag{10}$$

with the ratio $R(t) = S_\parallel(t)/S_\perp(t)$.

The expression in eq 10 describes the temporal evolution of the β_2 anisotropy parameter for two isoenergetic PE features arising from the photodetachment of an excited and ground state in a two-level system, when photodetachment is a one-photon process. It contains four unknown parameters: α, η, β_2^e, and τ. The ground state anisotropy, β_2^g, can be independently obtained as it corresponds to the measured value of β_2 when $t < 0$. In the limiting case when $\sigma^e = \sigma^g$, only three parameters are unknown because $\eta = 1$. It should also be noted that the parameter α may be extracted from pump power-dependence studies such that there would only be two remaining unknowns.

In the case of TCNQ$^-$ and the time-dependent anisotropy presented in Figure 5a, the higher energy feature around 2.0 eV may be used to obtain information about the parameters α and $\eta = \sigma^e/\sigma^g$. This feature originates from two-photon detachment of the D_0 ground state. With reference to Figure 4b, the parameter α, which is the fractional population transferred from the D_0 to the D_1 state, is equal to the ratio of the integrated signal (taken between 1.7 and 2.3 eV) of the 2.0 eV feature at $t = 0$, to the integrated signal of this feature before $t = 0$. This ratio yields a value of $\alpha = 0.5$.

The parameter $\eta = \sigma^e/\sigma^g$ can also be determined using a similar methodology in which the PE signal of the isoenergetic features at 0.2 eV is considered. Because the probe pulse for both components of this feature is the same, η is equivalent to the ratio of integrated intensities of the excited to ground state signals at $t = 0$:

$$\eta = \sigma^e/\sigma^g = S^g(t = 0)/S^e(t = 0) \tag{11}$$

With reference to Figure 4b, $S^g(t = 0)$ is obtained from the integrated area (from 0.15 to 0.25 eV) of the 0.2 eV feature before $t = 0$, scaled by the fractional population ($\alpha = 0.5$) that is transferred to the D_1 state following excitation. $S^e(t = 0)$ is then the integrated signal of the 0.2 eV feature at $t = 0$ with $S^g(t = 0)$ subtracted from it. Their ratio yields an estimate for the relative cross sections, $\eta = 7.4$. This value is in line with the observation that $\sigma^e > \sigma^g$ for TCNQ$^-$.

By extracting the parameters α, η, and β_2^g from the experimentally obtained time-resolved PE spectra, the number of free parameters in eq 10 have been reduced to the excited state anisotropy, β_2^e, and the desired D_1 excited state lifetime, τ. As the excited state lifetime is short and the observed dynamics may be influenced by the temporal resolution of the laser pulses ($\sim$120 fs), a convolution with Gaussian instrument response functions has been included in eq 5. The data in Figure 5a is fitted to eq 10 using a weighted least-squares fitting procedure, the result of which is shown as a solid black line in Figure 6. From the fit, an excited D_1 state lifetime of $\tau = 750 \pm 100$ fs is extracted, which is in reasonable agreement with the lifetime obtained from the temporally evolving signal in the time-resolved PE spectra ($\tau = 650 \pm 50$ fs).[8] The overall fit is good, but becomes poorer at longer times ($t > 2$ ps). The data (see Figure 5a) suggest that the anisotropy does not recover completely to the ground state value of $\beta_2 = -0.13$. Given the experimental uncertainty, this offset may not necessarily be real. However, there is some evidence from the PE signal at longer
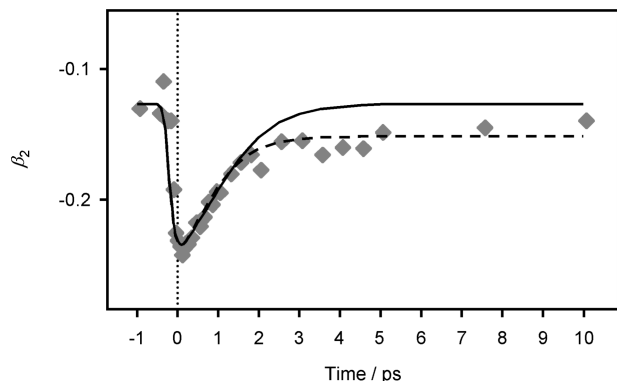
Ultrafast Relaxation Dynamics

J. Phys. Chem. A, Vol. 114, No. 42, 2010 **11223**

Figure 6. Results of the least-squares fitting procedure to the experimental β_2 data (Figure 5a) obtained from the isoenergetic features at 0.2 eV (gray diamonds). The black line shows the result of the fit using eq 10. The dashed black line shows the resultant fit when an offset between the final anisotropy ($t \gg 0$) and the original ground state anisotropy is introduced ($t < 0$) into eq 5.

times that it may be real. Specifically, we have previously shown that the dominant relaxation pathway of the excited state is through internal conversion, but at longer delays, there is evidence that a small fraction of the population remains in the excited state, evidenced by the fact that the 0.2 eV feature does not recover to the expected $t < 0$ signal level.[8] Such an offset may be included in the data analysis by assuming that not all the D_1 excited state population has decayed in eq 5. Fitting the data with this modification yields the dashed line in Figure 6, which accurately represents the observed anisotropy over the time scale monitored in this experiment. A value of $\tau = 600 \pm 100$ fs is extracted from this fit, which is within the experimental errors of the lifetime extracted from the TRPES experiments. In reality, this small fraction of D_1 state population is also decaying, but on a different time scale. Although this could be included in the analysis, it would introduce additional parameters causing the fit to become ambiguous. An alternative explanation for the long-time offset in anisotropy may be that the ground state is vibrationally highly excited following internal conversion. As PADs are sensitive to the ro-vibrational state from which the electron was removed,[30] the ground state anisotropy after internal conversion is not necessarily the same as that observed before excitation.

Despite these unknowns and the relatively large uncertainty in the measured anisotropy data, the main result from this study is that the lifetime extracted from a fit to the model provides strong support that population dynamics may be monitored through changes in PE anisotropy. The error bars on the data represent a single standard deviation and highlight the difficulty in obtaining high quality anisotropy parameters. This is a serious drawback of TRPEI; in general, it requires large amounts of data to produce high quality anisotropy measurements. On the other hand, signal stability is not an issue as this will only affect the relative error in obtaining an anisotropy parameter rather than the actual value. It should be noted that TCNQ$^-$ is a particularly favorable case in which certain fit parameters could be determined experimentally, thus reducing the number of free parameters required for the fitting procedure and ultimately making it more manageable. A least-squares fitting procedure in which all parameters are allowed to vary is very sensitive to their initial values.

In addition to the excited state lifetime, the fit to eq 10 also provides a measure for the D_1 excited state anisotropy, which is determined to be $\beta_2^e = -0.26$ for both fits presented in Figure 6. This value is slightly lower than the measured anisotropy at

$t = 0$ of the 0.2 eV feature ($\beta_2 = -0.23$), highlighting the remaining contribution of the ground state to this feature. In systems where the difference in anisotropies for the ground and excited states is more significant, the measured anisotropy may be very different from the actual anisotropy of the excited state.

The temporal evolution of the PE anisotropy defined by eq 10 provides a reasonable qualitative and quantitative description of the dynamics. However, it does rely on a number of approximations. (1) As the photoelectrons emitted are isoenergetic, the two PE waves will interfere with each other. This interference may manifest itself as a modulation on the energy spectrum[31] or may alter the observed PADs.[27] The latter will depend on the relative phases and amplitudes of outgoing partial waves formed. In the case of TCNQ$^-$, the amplitude of the excited state PE wave is much larger than that of the ground state ($\sigma^e > \sigma^g$), such that this dominates. However, in a scenario where $\sigma^e \approx \sigma^g$, the observed anisotropy does not necessarily provide information about the excited state anisotropy as the two PE waves can interfere. (2) There are no vibrational dynamics that lead to an energy shift in the PE spectrum with time or lead to changes in the symmetry of the orbital from which detachment occurs as the wave packet evolves. The latter is exemplified by the adiabatic dissociation dynamics of CS_2.[14] If there are changes in PE kinetic energy, the anisotropy may be modulated by the wavepacket dynamics. In TCNQ$^-$, there is evidence of wavepacket dynamics on the D_1 excited state;[8] however, the PE energy shift associated with this coherent motion is very small ($\sim$10 meV). (3) Only two states are involved in the relaxation and there is no internal vibrational relaxation (IVR) on the excited state. If any intermediate states are involved, the model presented would need to take into account the kinetics of the intermediate state, whether it contributed to the observed anisotropy or not. In the case of IVR on the excited state, this could change the PE anisotropy of the excited state as this is sensitive to ro-vibrational states.[30] Similarly, it is assumed that the ground state anisotropy is the same even though it will be highly vibrationally excited following internal conversion. In principle, this may be accounted for and may be used to provide further insight into the dynamics of IVR in the ground state.

V. Conclusions

A detailed description of a newly developed photoelectron imaging spectrometer has been presented. The instrument employs ESI as a source of anions. The continuous source of anions is coupled to a TOF mass-spectrometer using an RF ion guide, which is based on the principles of the ion funnel, and an ion trap incorporated in the same device. The trap can operate at several kilo-Hertz and can in principle convert the continuous ion beam into a pulsed source of ions with near unit efficiency. Currently, the efficiency is limited by space-charge effects because of the relatively small dimensions of the ion guide. Photoelectron imaging is performed using a VMI arrangement perpendicular to the ion propagation axis. The VMI setup is specifically designed to operate at low constant voltages, resulting in a very small angular deflection of the ion beam. Aberrations are compensated for by using a resistive glass tube which produces a smooth potential gradient between the acceleration and ground electrodes of a typical VMI arrangement. The ground electrode in our case is the front of the MCP-phosphor screen detector.

The dynamics of the TCNQ radical anion have been studied using time-resolved photoelectron imaging. The photoelectron images of TCNQ$^-$ reveal that the photodetachment for the

11224 *J. Phys. Chem. A, Vol. 114, No. 42, 2010*

Lecointre et al.

ground D_0 state and the excited D_1 state exhibit a negative anisotropy, which is explained using the s-p model developed by Sanov and co-workers. As these two photoelectron features occur at nearly the same energy, the consequences of isoenergetic photoelectron features in time-resolved photoelectron spectroscopy are considered. In TCNQ$^-$, the ground and excited state features exhibit different anisotropy parameters and the relaxation dynamics may be observed from the temporally evolving anisotropy parameter of this isoenergetic feature. A simple model based on the relative population dynamics parallel and perpendicular to the polarization axis is presented. The model allows the time-dependent anisotropy to be calculated and is used to fit to the experimentally observed dynamics. The fit yields good quantitative agreement with the dynamics extracted from the time-resolved photoelectron spectra and indicates that, despite the relatively simplistic nature of the model, temporally evolving anisotropy parameters can provide detailed insights into the population dynamics of complex molecular systems.

References and Notes

(1) Zewail, A. H. *J. Phys. Chem. A* **2000**, *104*, 5660.

(2) Stolow, A.; Bragg, A. E.; Neumark, D. M. *Chem. Rev.* **2004**, *104*, 1719.

(3) Muller-Dethlefs, K.; Schlag, E. W. *Angew. Chem., Int. Ed.* **1998**, *37*, 1346.

(4) Blanchet, V.; Zgierski, M. Z.; Seideman, T.; Stolow, A. *Nature* **1999**, *401*, 52.

(5) Verlet, J. R. R. *Chem. Soc. Rev.* **2008**, *37*, 505.

(6) (a) Bragg, A. E.; Verlet, J. R. R.; Kammrath, A.; Cheshnovsky, O.; Neumark, D. M. *Science* **2004**, *306*, 669. (b) Bragg, A. E.; Verlet, J. R. R.; Kammrath, A.; Cheshnovsky, O.; Neumark, D. M. *J. Am. Chem. Soc.* **2005**, *127*, 15283.

(7) (a) Nugent-Glandorf, L.; Scheer, M.; Samuels, D. A.; Mulhisen, A. M.; Grant, E. R.; Yang, X. M.; Bierbaum, V. M.; Leone, S. R. *Phys. Rev. Lett.* **2001**, *87*, 193002. (b) Nugent-Glandorf, L.; Scheer, M.; Samuels, D. A.; Bierbaum, V. M.; Leone, S. R. *J. Chem. Phys.* **2002**, *117*, 6108.

(8) Roberts, G. M.; Lecointre, J.; Horke, D. A.; Verlet, J. R. R. *Phys. Chem. Chem. Phys.* **2010**, *12*, 6226.

(9) (a) Worth, G. A.; Carley, R. E.; Fielding, H. H. *Chem. Phys.* **2007**, *338*, 220. (b) Parker, D. S. N.; Minns, R. S.; Penfold, T. J.; Worth, G. A.; Fielding, H. H. *Chem. Phys. Lett.* **2009**, *469*, 43.

(10) (a) Sanov, A.; Mabbs, R. *Int. Rev. Phys. Chem.* **2008**, *27*, 53. (b) Mabbs, R.; Grumbling, E. R.; Pichugin, K.; Sanov, A. *Chem. Soc. Rev.* **2009**, *38*, 2169.

(11) Seideman, T. *Annu. Rev. Phys. Chem.* **2002**, *53*, 41.

(12) Tsubouchi, M.; Whitaker, B. J.; Wang, L.; Kohguchi, H.; Suzuki, T. *Phys. Rev. Lett.* **2001**, *86*, 4500.

(13) Bragg, A. E.; Wester, R.; Davis, A. V.; Kammrath, A.; Neumark, D. M. *Chem. Phys. Lett.* **2003**, *376*, 767.

(14) Bisgaard, C. Z.; Clarkin, O. J.; Wu, G. R.; Lee, A. M. D.; Gessner, O.; Hayden, C. C.; Stolow, A. *Science* **2009**, *323*, 1464.

(15) Larsen, J. J.; Hald, K.; Bjerre, N.; Stapelfeldt, H.; Seideman, T. *Phys. Rev. Lett.* **2000**, *85*, 2470.

(16) (a) Schmitt, M.; Lochbrunner, S.; Shaffer, J. P.; Larsen, J. J.; Zgierski, M. Z.; Stolow, A. *J. Chem. Phys.* **2001**, *114*, 1206. (b) Farmanara, P.; Stert, V.; Radloff, W.; Hertel, I. V. *J. Phys. Chem. A* **2001**, *105*, 5613. (c) Davies, J. A.; Reid, K. L.; Towrie, M.; Matousek, P. *J. Chem. Phys.* **2002**, *117*, 9099. (d) Lee, S. H.; Tang, K. C.; Chen, I. C.; Schmitt, M.; Shaffer, J. P.; Schultz, T.; Underwood, J. G.; Zgierski, M. Z.; Stolow, A. *J. Phys. Chem. A* **2002**, *106*, 8979. (e) Schultz, T.; Quenneville, J.; Levine, B.; Toniolo, A.; Martinez, T. J.; Lochbrunner, S.; Schmitt, M.; Shaffer, J. P.; Zgierski, M. Z.; Stolow, A. *J. Am. Chem. Soc.* **2003**, *125*, 8098. (f) Blanchet, V.; Raffael, K.; Turri, G.; Chatel, B.; Girard, B.; Garcia, I. A.; Wilkinson, I.; Whitaker, B. J. *J. Chem. Phys.* **2008**, *128*, 164318.

(17) (a) Satzger, H.; Townsend, D.; Zgierski, M. Z.; Patchkovskii, S.; Ullrich, S.; Stolow, A. *Proc. Natl. Acad. Sci. U.S.A.* **2006**, *103*, 10196. (b) Gador, N.; Samoylova, E.; Smith, V. R.; Stolow, A.; Rayner, D. M.; Radloff, W. G.; Hertel, I. V.; Schultz, T. *J. Phys. Chem. A* **2007**, *111*, 11743.

(18) (a) Weber, J. M.; Ioffe, I. N.; Berndt, K. M.; Loffler, D.; Friedrich, J.; Ehrler, O. T.; Danell, A. S.; Parks, J. H.; Kappes, M. M. *J. Am. Chem. Soc.* **2004**, *126*, 8585. (b) Lee, I. R.; Lee, W.; Zewail, A. H. *Proc. Natl. Acad. Sci. U.S.A.* **2006**, *103*, 258.

(19) Fenn, J. B. *Angew. Chem., Int. Ed.* **2003**, *42*, 3871.

(20) (a) Wang, L. S.; Ding, C. F.; Wang, X. B.; Barlow, S. E. *Rev. Sci. Instrum.* **1999**, *70*, 1957. (b) Wang, X. B.; Yang, X.; Wang, L. S. *Int. Rev. Phys. Chem.* **2002**, *21*, 473. (c) Wang, X. B.; Wang, L. S. *Annu. Rev. Phys. Chem.* **2009**, *60*, 105.

(21) (a) Ehrler, O. T.; Yang, J. P.; Hattig, C.; Unterreiner, A. N.; Hippler, H.; Kappes, M. M. *J. Chem. Phys.* **2006**, *125*, 074312. (b) Ehrler, O. T.; Yang, J. P.; Sugiharto, A. B.; Unterreiner, A. N.; Kappes, M. M. *J. Chem. Phys.* **2007**, *127*, 184301. (c) Rensing, C.; Ehrler, O. T.; Yang, J. P.; Unterreiner, A. N.; Kappes, M. M. *J. Chem. Phys.* **2009**, *130*, 234306.

(22) Wyttenbach, T.; Kemper, P. R.; Bowers, M. T. *Int. J. Mass Spectrom.* **2001**, *212*, 13.

(23) Wiley, W. C.; Mclaren, I. H. *Rev. Sci. Instrum.* **1955**, *26*, 1150.

(24) Eppink, A. T. J. B.; Parker, D. H. *Rev. Sci. Instrum.* **1997**, *68*, 3477.

(25) Lin, J. J.; Zhou, J. G.; Shiu, W. C.; Liu, K. P. *Rev. Sci. Instrum.* **2003**, *74*, 2495.

(26) Roberts, G. M.; Nixon, J. L.; Lecointre, J.; Wrede, E.; Verlet, J. R. R. *Rev. Sci. Instrum.* **2009**, *80*, 053104.

(27) Cooper, J.; Zare, R. N. *J. Chem. Phys.* **1968**, *48*, 942.

(28) Wigner, E. P. *Phys. Rev.* **1948**, *73*, 1002.

(29) Brinkman, E. A.; Gunther, E.; Schafer, O.; Brauman, J. I. *J. Chem. Phys.* **1994**, *100*, 1840.

(30) Hockett, P.; Staniforth, M.; Reid, K. L.; Townsend, D. *Phys. Rev. Lett.* **2009**, *102*, 253002.

(31) Wollenhaupt, M.; Assion, A.; Liese, D.; Sarpe-Tudoran, C.; Baumert, T.; Zamith, S.; Bouchene, M. A.; Girard, B.; Flettner, A.; Weichmann, U.; Gerber, G. *Phys. Rev. Lett.* **2002**, *89*, 173001.